International Journal of
INTELLIGENT SYSTEMS AND APPLICATIONS IN ENGINEERING
ISSN:2147-6799 www.ijisae.org Original Research Paper

African Vulture Optimization with Deep Learning based Geographical Information Analytics for Land Cover Segmentation and Classification

[1]Anil Antony, [2]Ganesh Kumar R[2]

Submitted: 28/01/2024 **Revised**: 06/03/2024 **Accepted**: 14/03/2024

Abstract: Owing to the complications of LULC, the numerous kinds of seasonal variations, and human actions, Land use and land cover (LULC) become a challenge for monitoring and identification. Therefore, machine learning (ML) and Remote sensing (RS) technologies are employed to overcome these issues for generating LULC maps. RS identification uses object-based and pixel-based classifications which deliver LU classification with higher performance. However, this technique constantly needs sample data for parameter adjustment and training. ML has been instrumental in RS classification and has achieved remarkable outcomes for the LULC classification. Furthermore, currently, semantic segmentation is generally utilized in remote sensing images (RSI) for mapping crop types, glacial lakes, LC, and buildings. In the present scenario, Convolution Neural Networks (CNN) have attained more effective results for numerous tasks comprising LC estimates due to their capability to remove multiscale feature maps. The most complex issue in standard spatial resolution images is employing deep learning (DL) semantic segmentation for LU removal. Therefore, this study presents an optimum DL-based segmentation and classification method for LULC, termed the ODLSC-LULC approach. The segmentation stage uses U2Net, a strong DL-based segmentation system, to exactly describe spatial features and improve contextual understanding. The SE-ResNet architecture is employed for feature extraction, taking hierarchical representations of land features for more discriminative identification. To modify the model's parameters efficiently, we present the African Vulture Optimizer Algorithm (AVOA), which represents the foraging behavior of vultures to constantly enhance the network's configuration. At last, a Bidirectional Long Short-Term Memory (BiLSTM) classifier is utilized to analyze successive dependencies and safeguard the precise classification of different land cover classes. Experimental outcomes on benchmark datasets determine the better performance of ODLSC-LULC, showcasing its efficiency in attaining optimum classification and segmentation outcomes for difficult and dynamic LU scenarios.

Keywords: *Land Use and Land Cover; Remote Sensing Image; Deep Learning; Segmentation; African Vulture Optimizer Algorithm*

1. Introduction

Land Use Land Cover (LULC) classification is important in remote sensing (RS) and environment monitoring [1]. It involves categorizing the Earth's surface into several groups that depend upon the various types of LC like agriculture, water bodies, urban regions, forests, and so on. These details are needed for different applications, comprising disaster assessment, agricultural management, urban planning, and natural resource conservation [2]. Improving accessibility of remotely sensed images because of the fast development of RS technology increases the horizon of the selections of image sources. The accessible sources have been identified for their changes in temporal, radiometric, spectral, and spatial resolutions so that will be appropriate for various objectives [3]. RS data or information obtained through satellite sensors offer incessant datasets that could be employed for identifying and monitoring various earth phenomena. It has been utilized for measuring the types of environmental parameters namely surface and cloud top reflectance, regions and possible yield of specified crop varieties, density and height of forest stands, snow and water content, soil, and fraction of photosynthetic active radiation [4].

High spatial resolution images are about 30 cm to 10 m and can be proficient in extracting and classifying complex LULC features to be unnoticed in medium or lower-resolution imageries [5]. The resolution can be higher prospective for the LULC classification categories as described in the LULC Level-3 classification model. Such types of image resolutions can be mainly categorized by image processing employing machine learning (ML) techniques. ML has performed a significant part in RS classification for more than ten years and provides excellent effectiveness for LULC classification [6]. The pixel-and object-based classifications are implemented by ML methods like random forest (RF), K-nearest neighbor (KNN), support vector machine (SVM), decision tree (DT), and maximum likelihood estimator (MLE) [7]. Currently, deep learning (DL) techniques are a vast and useful attention for automated classification of RSI. They manage the big data issues and the difficulty of LU characteristics. These

[1]*Department of Computer Science & Engineering, CHRIST (Deemed to be University), School of Engineering and Technology Kengeri Campus, Bangalore – 560074 ORCID ID : 0000-0003-0476-8167*
[2]*Department of Computer Science & Engineering, CHRIST (Deemed to be University), School of Engineering and Technology Kengeri Campus, Bangalore – 560074 ORCID ID : 0000-0001-7817-1019*
[1] *anil.antony@res.christuniversity.in and* [2]*ganesh.kumar@christuniversity.in*
**Corresponding Author: Anil Antony. Email: anil.antony@res.christuniversity.in*

methods are employed for object segmentation and image classification and have been demonstrated more effective for numerous RS applications. LULC classification and DL semantic segmentation techniques have been a quickly developing research advancement [8]. According to the study, the study shows that DL semantic segmentation can identify and extract the variabilities and intricacy of LU features precisely [9]. On the other hand, the baseline network substructure that has been employed for the supervised learning method has deep and intricate convolution layers for learning under multidimensional data, and LU characteristics above medium spatial resolution imageries have middle-level features [10].

The ODLSC-LULC approach utilizes U2Net for precise spatial feature description during segmentation, while SE-ResNet extracts hierarchical LULC features for enhanced identification. The African Vulture Optimizer Algorithm efficiently adjusts model parameters, followed by classification using a Bidirectional Long Short-Term Memory (BiLSTM) classifier, demonstrating superior performance in challenging land use scenarios.

2. Literature Survey

Li et al. [11] developed a DL technique of surface complexity exploration that is dependent upon multiscale entropy. The technique could be employed to decrease the entropy-based invariance and sampling bias to learn the semantic segmentation of LULC images. The quantitative systems efficiently recognized and removed local surface complexity scores, representing their wide-ranging utility. In [12], LULC mapping has been implemented by employing the developed CNN–MRS technique. Various types of Sentinel-2A images and diverse patch sizes have been utilized in the primary analysis. Yu et al. [13] designed an integrated CNN named DUA-Net architecture. The DUA-Net incorporated UNet and Densely connected Atrous Spatial Pyramid Pooling (DenseASPP) for extracting RSI features in parallel. Subsequently, the channel attention mechanism has been employed to proficiently combine the multi-source semantic data at the double-layer model output. Lastly, LULC classification of higher-resolution urban RSI could be accomplished.

In [14], an innovative multimodal DL method was developed by encompassing traditional ViT with decreased variations. This method can process the multimodal RSI patches with equivalent divisions of position-divided ViTs comprehensively with separate convolution components. Additionally, their tokenized embeddings have been combined across cross-modality attention (CMA) components by utilizing pixel-level spatial relationships in RSI. Xu et al. [15] presented an enriched classification technique including Recurrent Neural Network (RNN) system with RF algorithm for LU classification employing satellite images that have been openly accessible for diverse research. The technique employed the spatial data collected from the satellite images like time series. The employed experimental classification was dependent upon object-based classification and pixel. Cheng et al. [16] presented a multi-level LC contextual (MLCC) algorithm that must be flexibly combined with the efficient global context with local context for categorizing LC. The MLCC model encompasses 2 components first one is a DCNN-based LC classification network (DLCN) and another one is multiple-level context integration module (MCIM). Also, MCIM permits the incorporation of the global and local contexts in the direction of uncertainty mapping in a resourceful process.

In [17], a CNN method dependent upon the LeNet model was developed for executing the LULC classification through Sentinel-2 images. The CNN techniques like LeNet need decreased computation efficiency related to highly complicated models. An entire 11 LULC classes will be employed for validating and training the system that can be then employed for categorizing the sub-basins. Castelo-Cabay et al. [18] introduced a classification of the LULC by employing satellite images through numerous classifiers and found which of them achieved the better efficiency for which three various techniques were implemented such as Deep Neural Network (DNN), Geographic Object-Based Image Analysis (GEOBIA), and Pixel-Based Image Analysis (PBIA). Different factors and seven categories have been employed.

."

3. The Proposed Model

In this study, we have established an optimum DL-based segmentation and classification method for LULC, termed the ODLSC-LULC approach. The main purposes of the ODLSC-LULC approach are four different processes involved U2Net-based segmentation, SE-ResNet-based feature extractor, AVOA-based hyperparameter tuning, and BiLSTM-based classification process. Fig. 1 demonstrates the entire flow of the ODLSC-LULC algorithm.

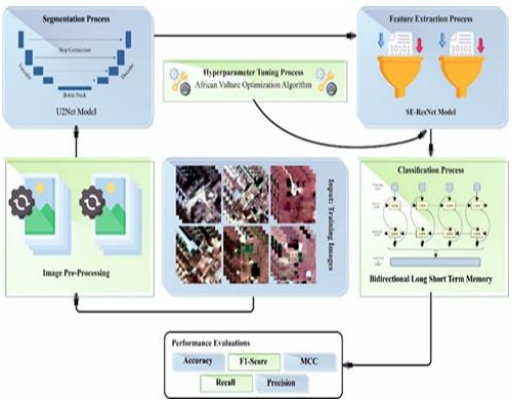

Fig. 1. Overall flow of the ODLSC-LULC method

3.1. Segmentation Process

At the primary level, the ODLSC-LULC approach takes place segmentation process using the U2Net model. The improvement of the U2Net method is its design, and capability to adjust to dissimilar areas and modify the function of loss [19]. Inserting color data into the technique along with generating novel dissimilar convolutional (Conv) layers and combining it with flattened and dense layers permits the U2Net method to take different visual prompts of diverted driving and improve the outcomes of identification. U2Net enhances the power of the entire UNet structure without extensively enhancing the computation cost due to pooling processes.

The U2-net method modifies the UNet structure by incorporating 4 additional Conv layers and 2 max-pooling layers in the contracting pathway, while also expanding 2 max-pooling layers and 4 upsampling layers in the expanding pathway, facilitating spatial data integration and increasing output resolution. By downsizing input images to 256×256 dimensions and employing Conv processes followed by pooling functions, the model enhances localization and reduces training time, with transpose Conv layers subsequently upsampling to predict feature maps and enhance resolution for effective planning and context recognition in the network's architecture.

3.2. SE-ResNet-based Feature Extractor

The SE-ResNet can be employed for the feature extraction process. CNN has presented its power in computer visual challenges [20]. The SE block enhances representative features by recalibrating network features automatically, utilizing weight acquisition through learning. Employing global average pooling, the squeeze operator reduces input data, while the excitation process, incorporating dual fully connected layers with ReLU activation, emphasizes input data to generate weight channels, optimizing feature extraction in tasks such as image detection and classification through the SE-ResNet model's integration of SE blocks with ResNet residual blocks. We increase the SE-ResNet output in Eq. (1).

$$y=F(f\_se\ (x),(\omega\_i\ ))+x \quad (1)$$

Whereas ω_i refers to the weight of the i^th input, f_se (·) represents the function of the SE block, and y, and x denote the output and input of the SE-ResNet, correspondingly. However, in the squeeze operator process, we want to describe the feature image scale, which will significantly change the re-weight value. Meanwhile, the dimensions of input features are not similar, this study offers a variable scale as per the feature channel size. We describe the j^th output of SE-ResNet as in Eq. (2).

$$y\_j=F(f\_se\ (x\_j\ ),(\omega\_ij\ ))+x\_j \quad (2)$$

Here y_j represents the jth output of SE-ResNet. Fig. 2 describes the architecture of SE-ResNet.

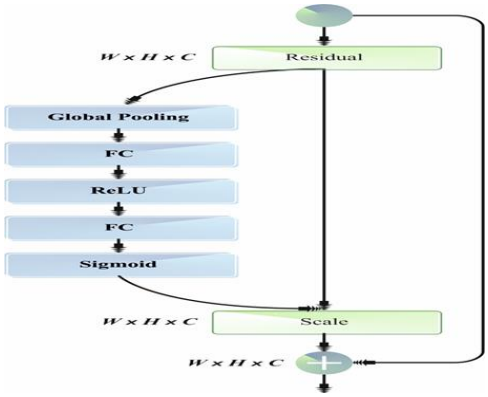

Fig. 2. Architecture of SE-ResNet.

3.3. Hyperparameter Tuning Process

The AVOA method is applied for the optimal hyperparameter tuning related to the SE-ResNet approach. AVOA is a new nature-based algorithm that pretends to the uncommon behaviors of African vultures in foraging and navigation [21].

A). Formation of Population

After being set by population of N, vultures have been separated into 3 groups dependent upon estimated fitness value. The vulture group with the optimal solution, and then the finest solutions are stored in the 2nd group and remain retained in the 3rd group. Eq. (3) is projected in order to define which vulture must be shifted to the existing iteration:

$$R(i) = \begin{Bmatrix} Best_{Vulture1} if\ pi = L1 \\ Best_{Vulture2} if\ pi = L2 \end{Bmatrix} \quad (3)$$

Here, pi is defined utilizing the roulette wheel model; L2 and L1 denote the random numbers among the range of [0,1], with sum equivalent to 1.

B). Starvation assignment

The satiation and hunger phenomena such as insufficient energy, and violent seeking for foodstuff are imitated by Eqs. (4) and (5):

$$t = h^{*}(\sin^{w}(\pi/2 * i/\max_i) + \cos(\pi/2i/\max_i) - 1) \quad (4)$$

$$F = (2^{*}rand_1 + 1)^{*}z^{*}\left(1 - \frac{iter\_i}{\max_i}\right) + t \quad (5)$$

Whereas max_i represents the maximum iterations count, Iter_- i means existing iteration, z is the random number among -l and 1, F signifies vulture satiation which selects the search model of vulture in exploitation or exploration

mode, h is the arbitrary number among -2 and 2, and rand_1 refers to the random number amongst zero and one.

C). Exploration

At this stage, starving vultures (F>1) are directed to discover more united solutions in diverse random regions by picking the exact plan between dual as definite by the parameter Pl [0 and 1] at Eq. (6). If P1>1, the Eq. (7) is utilized or else Eq. (9) is employed to perfect this event:

$$v(i+1) = \begin{Bmatrix} Eq.(7)\ if\ P_1 \geq randP1 \\ Eq.(9)\ if\ P_1 < randP1 \end{Bmatrix} \quad (6)$$

$$v(i+1) = R(i) - D(i) * F \quad (7)$$

$$D(i) = X * R(i) - v(i) \quad (8)$$

Whereas v(i+1) denotes the location vector of the vulture in the next iteration. Eq. (8) signifies the food search near the finest vultures at random distances (i). X is employed as a co-efficient vector in every iteration, which is attained by the formulation X=2×rand [0 and 1].

$$v(i+1) = v(i) - F + rand2 * \big((ub - lb) * rand3 + lb\big) \quad (9)$$

While, lb and ub are the lower and upper bound of the variables, rand3 ranges among [0 and 1].

D). Exploitation

Vultures with F value which is larger than one arrive to develop the search area with two dissimilar tactics in every stage. Parameters P_3 and P_2 are employed to pick the plans accessible in the 1st and 2nd phases correspondingly. The AVOA goes into the exploitation of 1st phase when the value |F| lies among 1 and 0.5 or else the AVOA will follow the 2nd phase. In the 1st stage, twofold dissimilar rotating flight and *siege-flight* approaches have been implemented according to Eq. (10) which is given below:

$$v(i+1) = \begin{Bmatrix} Eq.(11)\ if\ P_2 \geq randP2 \\ Eq.\ (14)\ if\ P_2 < randP2 \end{Bmatrix} \quad (10)$$

Strategy 1: Siege and Food Competition

The weaker vultures attempt to exhaust and acquire foods from healthy predators by collecting nearby them and making little fights.

$$v(i+1) = D(i) * (F + rand_4) - d(t) \quad (11)$$

$$d(i) = R(i) - v(i) \quad (12)$$

Upgraded vulture location is v(i+1) and rand_4 denotes the random integer within [0,1], which is utilized to enlarge the arbitrary co-efficient.

Strategy 2: Rotational Spiral Flight Mode

This stage is employed to perfect the rotating flight of predators. A formulation of the spiral has been produced between all vultures as well as one of the dual finest vultures. The S_1 and S_2 accepted by predators is stated utilizing Eq. (13):

$$\left.\begin{aligned} S_1 &= R(i) * \left(\frac{rand_5 * v(i)}{2\pi}\right) * \cos\big(v(i)\big) \\ S_2 &= R(i) * \left(\frac{rand_3 * v(i)}{2\pi}\right) \sin\big(v(i)\big) \end{aligned}\right\} \quad (13)$$

$$v(i+1) = R(i) - (S_1 + S_2) \quad (14)$$

At last, by employing Eq. (14), the position of vultures is upgraded.

Phase 2: Vulture movement near the food basis is inspected at this stage. To define the range of every strategy, the parameter P_3 is utilized in Eq. (15) which is as follows, whereas randP3 is a random number among 0 and 1.

$$v(i+1) = \begin{Bmatrix} Eq.(18)\ if\ P_3 \geq randP3 \\ Eq.\ (19)\ if\ P_3 < randP3 \end{Bmatrix} \quad (15)$$

Strategy 3: Gathering of vulture species around food

Numerous kinds of vulture species obtain stored over food and fight for foodstuff.

Utilizing Eqs. (16) and (17), the accumulation of the vulture's movement is demonstrated:

$$A_1 = Bestvulturel\ (i) - D(i) \times F \quad (16)$$

$$A_2 = Bestvulture2(i) - D(i) \times F \quad (17)$$

$$v(i+1) = \frac{A_1 + A_2}{2} \quad (18)$$

A2 and A_1 denote the location vector of the vulture. Therefore, the accumulation of all vultures is implemented by utilizing Eq. (18).

Strategy 4: Aggressive Competition for Food

Once AVOA takes place, then food lack will be started. So, they collect food in every place and perform reasonably. They used to follow dissimilar guiding movements by assuming levy flight events and heading near the foremost

predator. This kind of behavior is demonstrated below

$$v(i+1) = R(i) - |d(i)| * F * Levy(d) \quad (19)$$

Whereas d(i) signifies the vulture distance and intended employing Eq. (25). The levy flight patterns are applied in order to enhance the efficacy of AVOA.

The AVOA method is used to derive an FF for achieving high classifier accuracy. It determines a positive integer to epitomize the better efficiency of the solution candidate. Here, the minimization of classifier errors is assumed as FF.

$$fitness(x_i) = ClassifierErrorRate(x_i) = \frac{No.of\ misclassified\ samples}{Total\ No.of\ samples} * 100 \quad (20)$$

3.4. Classification using the Bi-LSTM Model

At last, the Bi-LSTM model can utilized for the detection and classification of different LC classes. Recurrent neural network (RNN) reflects the relation characteristics of time sequence [22]. The extraction of prior data for the stock market is limited due to gradient explosion or disappearance problems. LSTM-NN is a kind of RNN that has significant benefits in handling the long-term dependency of time-sequence data. LSTM is an extension of RNN, which includes input, forget, and output gates. The integral scale at dissimilar times is changed dynamically once the parameter model is fixed, which efficiently resolves the vanishing or exploding gradients and the existence of RNN problems.

Initially, the forget gate f_t decides what data should be removed from the cell.

$$f_t = \sigma(b_f + W_f x_t + U_f h_{t-1}) \quad (21)$$

Where the bias, the input weight, and the loop weight of the forget gate are represented as b_f, Wf, U_f, correspondingly. x_i denotes the existing input vector σ indicates the sigmoid activation function and h_t represents the HL vectors.

Consider external input gate g_t within [0,1] is subject to the sigmoid function:

$$g_t = \sigma(b_g + W_g x_t + U_g h_{t-1}) \quad (22)$$

Next, the cell state C_t is updated according to C_(t-1) as follows

$$C_t = f_t C_{t-1} + g_t \tanh(b_c + W_c x_t + U_c h_{t-1}) \quad (23)$$

Lastly, the data output h_t=o_t*tanh(C_t) is subject to the input gate and it is described by:

$$o_t = \sigma(b_o + W_o x_t + U_o h_{t-1}) \quad (24)$$

The Bi-LSTM-NN composed of two LSTM-NN, receives a similar input. It can be trained in forward and backward directions with LSTM-NN deciding on the last output.

$$h_t = f(w_1 X_t + w_2 h_{t-1}) \quad (25)$$

$$h_t = f(w_3 X_t + w_5 h_{t+1}) \quad (26)$$

$$o_t = g(w_4 h_t + w_6 h_t') \quad (27)$$

Where,w_1,w_2,w_3,w_4,w_5, and w_6 denote the weight matrices, X_t indicates the input at the moment, h_t implies the output at the forward layer at the moment, $h_{t^\wedge}$' means the output at the reverse layer at the moment, $h_{(t-1)}$ refers to the output at prior moment, 0_t signifies the output at the moment, and $h_{(t+1)}$ shows the output at next time.

4. Experimental Validation

The stimulation analysis of the ODLSC-LULC algorithm is tested using the Sen-2 LULC dataset [23]. It includes 1750 samples with 7 class labels as illustrated in Table 1.

Table 1: Details of database

Classes	**No. of Samples**
Water Bodies	250
Dense Forest	250
Built up	250
Agriculture land	250
Barren land	250
Fallow land	250
Sparse Forest	250
Total Samples	**1750**

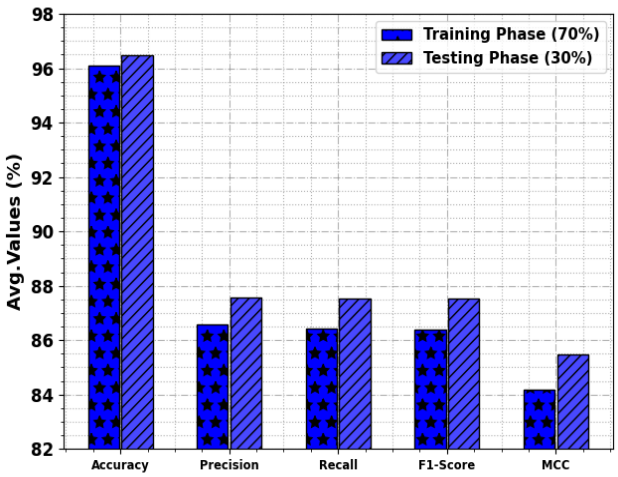

Fig. 3. Average of ODLSC-LULC method on 70:30 of TRAPH/TESPH

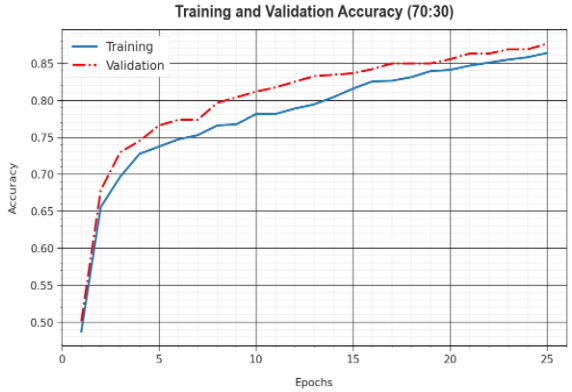

Fig. 4. $Accu_y$ curve of ODLSC-LULC technique under 70:30 of TRAPH/TESPH

The performance of the ODLSC-LULC technique on 70:30 of TRAPH/TESPH is depicted in Fig. 3 through TRAA and VALA curves, illustrating its learning process and generalization abilities across epochs, with a notable steady improvement in both metrics suggesting its adaptive nature in pattern recognition. Additionally, Fig. 4 presents the TRLA and VALL outcomes, showing the ODLSC-LULC model's ability to reduce classifier error and capture patterns within the datasets, with continuous parameter enhancement aiming to minimize differences between predicted and actual class labels in the training data.

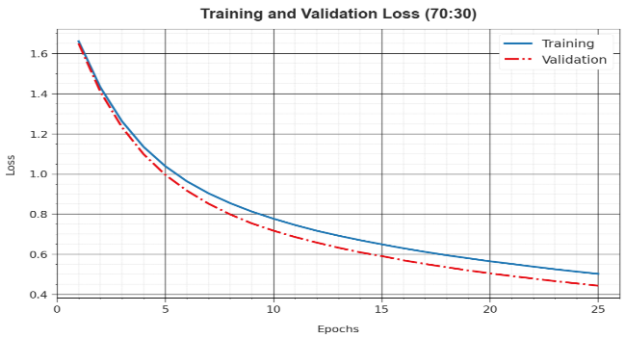

Fig. 5. Loss curve of ODLSC-LULC technique on 70:30 of TRAPH/TESPH

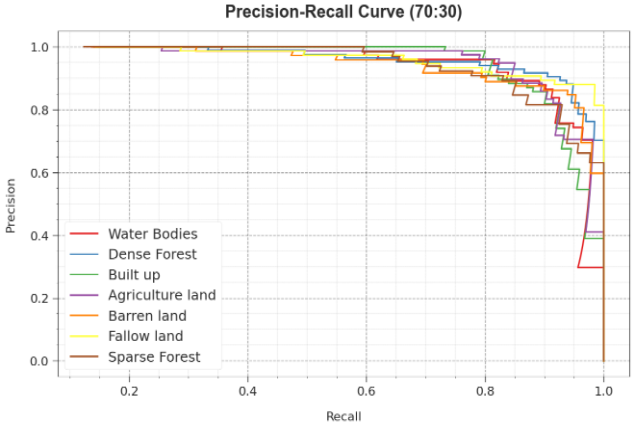

Fig. 6. PR curve of ODLSC-LULC technique under 70:30 of TRAPH/TESPH

Inspecting the PR curve, as displayed in Fig. 6, the results ensured that the ODLSC-LULC model on 70:30 of TRAPH/TESPH progressively accomplishes better PR values under each class. It verifies the improved abilities of the ODLSC-LULC technique in the detection of distinct classes, exhibiting proficiency in the recognition of classes.

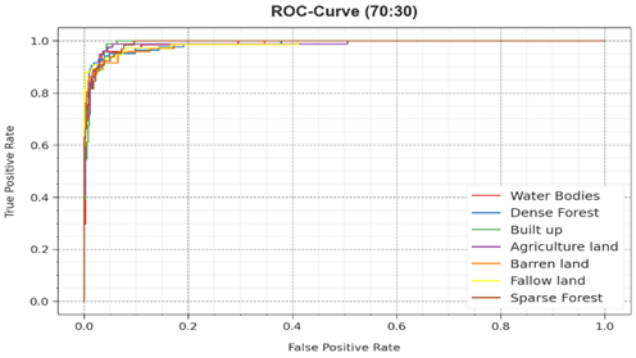

Fig. 7. ROC curve of ODLSC-LULC technique under 70:30 of TRAPH/TESPH

At last, a brief comparison study is made with recent approaches on LULC in Table 2 and Fig. 8 [23-25]. The outcomes infer that the CNN-SVM, CNN-RF, DeeplabV3+, and LoopNet models have resulted in poor performance. Meanwhile, the UNet-ResNet50, UNetResNet101, and UNet-ResNet152 models have reached closer results. Nevertheless, the ODLSC-LULC technique gains maximum performance with accu_y, prec_n, reca_l, and F1_{score} of 96.49%, 87.65%, 87.02%, and 87.22%, respectively. Therefore, the ODLSC-LULC method can be applied for automated segmentation and classification of LULC.

Table 3 Comparative outcome of ODLSC-LULC technique with existing algorithms

Method	$Accu_y$	$Prec_n$	$Reca_l$	$F1_{Score}$
CNN-SVM Model	82.06	81.08	82.08	81.06
CNN-RF Model	83.06	83.08	83.07	82.06
DeeplabV3+	85.18	87.01	86.57	66.24
LoopNet Model	89.90	87.03	86.86	71.74
UNet-ResNet50	95.05	73.07	68.06	70.08
UNet-ResNet101	95.06	69.06	67.07	68.06
UNet-ResNet152	95.07	73.08	68.06	70.06
ODLSC-LULC	96.49	87.65	87.02	87.22

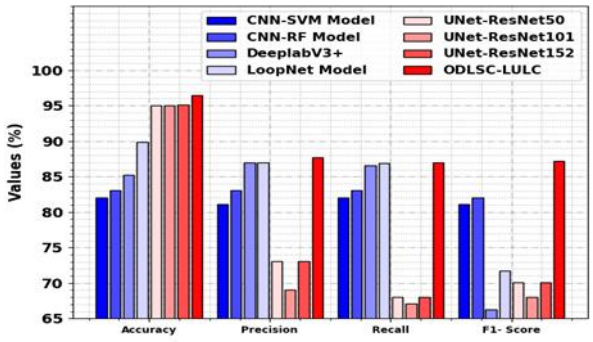

Fig. 8. Comparative outcome of ODLSC-LULC technique with existing algorithms

4. Conclusion

A conclusion In this study, we have developed an optimum DL-based segmentation and classification method for LULC, termed the ODLSC-LULC approach. The main purposes of the ODLSC-LULC approach are four different processes U2Net U2Net-based segmentation, SE-ResNet-based feature extractor, AVOA-based hyperparameter tuning, and BiLSTM-based classification process. The segmentation stage uses U2Net, a strong DL-based segmentation system, to exactly describe spatial features and improve contextual understanding. The SE-ResNet architecture is employed for feature extraction, taking hierarchical representations of land features for more discriminative identification. To modify the model's parameters efficiently, we present the AVOA, which represents the foraging behavior of vultures to constantly enhance the network's configuration. At last, a Bi-LSTM classifier is utilized to analyze successive dependencies and safeguard the precise classification of different land cover classes. Experimental outcomes on benchmark datasets determine the better performance of ODLSC-LULC, showcasing its efficiency in attaining optimum classification and segmentation outcomes for difficult and dynamic land use scenarios.

References

[1] Suryawanshi, P., Sawant, S. and Joshi, A., 2023. Land use Land Cover Classification using Deep Neural Network. Grenze International Journal of Engineering & Technology (GIJET), 9(1).

[2] Sertel, E., Ekim, B., Ettehadi Osgouei, P. and Kabadayi, M.E., 2022. Land use and land cover mapping using deep learning-based segmentation approaches and vhr worldview-3 images. Remote Sensing, 14(18), p.4558.

[3] Rousset, G., Despinoy, M., Schindler, K. and Mangeas, M., 2021. Assessment of deep learning techniques for land use land cover classification in southern New Caledonia. Remote Sensing, 13(12), p.2257.

[4] Papoutsis, I., Bountos, N.I., Zavras, A., Michail, D. and Tryfonopoulos, C., 2023. Benchmarking and scaling of deep learning models for land cover image classification. ISPRS Journal of Photogrammetry and Remote Sensing, 195, pp.250-268.

[5] Saralioglu, E. and Gungor, O., 2022. Semantic segmentation of land cover from high-resolution multispectral satellite images by spectral-spatial convolutional neural network. Geocarto International, 37(2), pp.657-677.

[6] Tzepkenlis, A., Marthoglou, K. and Grammalidis, N., 2023. Efficient Deep Semantic Segmentation for Land Cover Classification Using Sentinel Imagery. Remote Sensing, 15(8), p.2027.

[7] Zhang, W., Tang, P. and Zhao, L., 2021. Fast and accurate land-cover classification on medium-resolution remote-sensing images using segmentation models. International Journal of Remote Sensing, 42(9), pp.3277-3301.

[8] Mehra, A., Jain, N. and Srivastava, H.S., 2022. A novel approach to use semantic segmentation-based deep learning networks to classify multi-temporal SAR data. Geocarto International, 37(1), pp.163-178.

[9] Horry, M.J., Chakraborty, S., Pradhan, B., Shulka, N. and Almazroui, M., 2023. Two-Speed Deep-Learning Ensemble for Classification of Incremental Land-Cover Satellite Image Patches. Earth Systems and Environment, 7(2), pp.525-540.

[10] Ali, K. and Johnson, B.A., 2022. Land-Use and Land-Cover Classification in Semi-Arid Areas from Medium-Resolution Remote-Sensing Imagery: A Deep Learning Approach. Sensors, 22(22), p.8750.

[11] Li, L., Zhu, Z. and Wang, C., 2023. Multiscale Entropy-Based Surface Complexity Analysis for Land Cover Image Semantic Segmentation. Remote Sensing, 15(8), p.2192.

[12] Atik, S.O. and Ipbuker, C., 2021. Integrating convolutional neural network and multiresolution segmentation for land cover and land use mapping using satellite imagery. Applied Sciences, 11(12), p.5551.

[13] Yu, J., Zeng, P., Yu, Y., Yu, H., Huang, L. and Zhou, D., 2022. A Combined Convolutional Neural Network for Urban Land-Use Classification with GIS Data. Remote Sensing, 14(5), p.1128.

[14] Yao, J., Zhang, B., Li, C., Hong, D. and Chanussot, J., 2023. Extended Vision Transformer (ExViT) for Land Use and Land Cover Classification: A Multimodal Deep Learning Framework. IEEE Transactions on Geoscience and Remote Sensing.

[15] Xu, X., Chen, Y., Zhang, J., Chen, Y., Anandhan, P. and Manickam, A., 2021. A novel approach for scene classification from remote sensing images using deep learning methods. European Journal of Remote Sensing, 54(sup2), pp.383-395.

[16] Cheng, X., He, X., Qiao, M., Li, P., Hu, S., Chang, P. and Tian, Z., 2022. Enhanced contextual representation with deep neural networks for land cover classification based on remote sensing images. International Journal of Applied Earth Observation and Geoinformation, 107, p.102706.

[17] Arrechea-Castillo, D.A., Solano-Correa, Y.T., Muñoz-Ordóñez, J.F., Pencue-Fierro, E.L. and Figueroa-Casas, A., 2023. Multiclass Land Use and Land Cover Classification of Andean Sub-Basins in Colombia with Sentinel-2 and Deep Learning. Remote Sensing, 15(10), p.2521.

[18] Castelo-Cabay, M., Piedra-Fernandez, J.A. and Ayala, R., 2022. Deep learning for land use and land cover classification from the Ecuadorian Paramo. International Journal of Digital Earth, 15(1), pp.1001-1017.

[19] Alsrehin, N.O., Gupta, M., Alsmadi, I. and Alrababah, S.A., 2023. U2-Net: A Very-Deep Convolutional Neural Network for Detecting Distracted Drivers. Applied Sciences, 13(21), p.11898.

[20] He, J. and Jiang, D., 2021. Fully automatic model based on se-resnet for bone age assessment. IEEE Access, 9, pp.62460-62466.

[21] Mishra, S. and Shaik, A.G., 2024. Solving Bi-objective economic-emission load dispatch of diesel-wind-solar microgrid using African vulture optimization algorithm. Heliyon.

[22] Aamir, M., Bhatti, M.A., Bazai, S.U., Marjan, S., Mirza, A.M., Wahid, A., Hasnain, A. and Bhatti, U.A., 2022. Predicting the Environmental Change of Carbon Emission Patterns in South Asia: A Deep Learning Approach Using BiLSTM. Atmosphere, 13(12), p.2011.

[23] Sawant, S., Garg, R.D., Meshram, V. and Mistry, S., 2023. Sen-2 LULC: Land uses land cover dataset for deep learning approaches. Data in Brief, 51, p.109724.

[24] Boonpook, W., Tan, Y., Nardkulpat, A., Torsri, K., Torteeka, P., Kamsing, P., Sawangwit, U., Pena, J. and Jainaen, M., 2023. Deep Learning Semantic Segmentation for Land Use and Land Cover Types Using Landsat 8 Imagery. ISPRS International Journal of Geo-Information, 12(1), p.14.

[25] Lilay, M.Y. and Taye, G.D., 2023. Semantic segmentation model for land cover classification from satellite images in Gambella National Park, Ethiopia. SN Applied Sciences, 5(3), p.76.